Human Molecular Genetics, 2012, Vol. 21, No. 18 **4060–4072**
doi:10.1093/hmg/dds230
Advance Access published on June 16, 2012

Apn1 AP-endonuclease is essential for the repair of oxidatively damaged DNA bases in yeast frataxin-deficient cells

Sophie Lefevre[1,2,†], Caroline Brossas[1], Françoise Auchère[1], Nicole Boggetto[3], Jean-Michel Camadro[1,*] and Renata Santos[1,*,‡]

[1]Institut Jacques Monod, CNRS-Université Paris Diderot, Sorbonne Paris Cité, 15 rue Hélène Brion, 75205 Paris cedex 13, France, [2]ED515 UPMC, 4 place Jussieu, 75005 Paris, France and [3]ImagoSeine Bioimaging Core Facility, Institut Jacques Monod, 15 rue Hélène Brion, 75205 Paris cedex 13, France

Received March 30, 2012; Revised and Accepted June 9, 2012

Frataxin deficiency results in mitochondrial dysfunction and oxidative stress and it is the cause of the hereditary neurodegenerative disease Friedreich ataxia (FA). Here, we present evidence that one of the pleiotropic effects of oxidative stress in frataxin-deficient yeast cells (Δ*yfh1* mutant) is damage to nuclear DNA and that repair requires the Apn1 AP-endonuclease of the base excision repair pathway. Major phenotypes of Δ*yfh1* cells are respiratory deficit, disturbed iron homeostasis and sensitivity to oxidants. These phenotypes are weak or absent under anaerobiosis. We show here that exposure of anaerobically grown Δ*yfh1* cells to oxygen leads to down-regulation of antioxidant defenses, increase in reactive oxygen species, delay in G1- and S-phases of the cell cycle and damage to mitochondrial and nuclear DNA. Nuclear DNA lesions in Δ*yfh1* cells are primarily caused by oxidized bases and single-strand breaks that can be detected 15–30 min after oxygen exposition. The Apn1 enzyme is essential for the repair of the DNA lesions in Δ*yfh1* cells. Compared with Δ*yfh1*, the double Δ*yfh1*Δ*apn1* mutant shows growth impairment, increased mutagenesis and extreme sensitivity to H_2O_2. On the contrary, overexpression of the *APN1* gene in Δ*yfh1* cells decreases spontaneous and induced mutagenesis. Our results show that frataxin deficiency in yeast cells leads to increased DNA base oxidation and requirement of Apn1 for repair, suggesting that DNA damage and repair could be important features in FA disease progression.

INTRODUCTION

Friedreich ataxia (FA) is the most common autosomal recessive inherited ataxia. This slowly progressive disease is characterized by neuron degeneration in the central and peripheral nervous system, cardiomyopathy and diabetes. FA is caused by a dynamic mutation in the *FXN* gene. The majority of patients are homozygous for a GAA trinucleotide repeat expansion in the first intron of the *FXN* gene that causes transcriptional silencing and low level of the encoded protein, frataxin (1–3). Frataxin is a mitochondrial protein implicated in iron–sulfur cluster biogenesis, iron homeostasis and resistance to oxidants (4–6). Convincing evidence show now that the primary function of frataxin is in Fe–S cluster biogenesis (7–9); however, oxidative stress seems to be the major pathological feature of the disease and the driving force that results in mitochondrial dysfunction and neuron degeneration (6,10).

One of the consequences of mitochondrial dysfunction and increase in reactive oxygen species (ROS) is the formation of nuclear and mitochondrial genome lesions (11). DNA damage

*To whom correspondence should be addressed at: Laboratory Mitochondria, Metals and Oxidative Stress, Institut Jacques Monod, Bât. Buffon, 15 rue Hélène Brion, 75205 Paris cedex 13, France. +33 157278029. Email: rsantos@biologie.ens.fr (R.S.); camadro.jean-michel@ijm.univ-paris-diderot.fr (J.M.C.)
†Present address: Molecular Cell Biology Group, GBB – University of Groningen, Nijenborgh 7, 9747 AG Groningen, The Netherlands.
‡Present address: Development of the Nervous System, IBENS, Ecole Normale Supérieure, 46 rue d'Ulm, 75230 Paris cedex 05, France.

is implicated in the common aging process, but deficiencies in the DNA repair pathways can result in cancer and neurodegeneration (12). Mitochondrial and nuclear DNA damage have been reported in human, mouse and yeast (Δ*yfh1* mutant) frataxin-deficient cells (13–16). Loss of mitochondrial DNA was one of the first phenotypes reported for the Δ*yfh1* yeast cells (17–19) and for FA patient cells (20). Thirty years ago, it was found that skin fibroblasts from FA patients were sensitive to ionizing radiation and that the newly synthesized DNA was abnormal, which were suggestive of defects in DNA repair. Recently, transcriptome profiling of total blood from 28 children with FA revealed the molecular signature of cell response to DNA damage (16). Using quantitative PCR, the same authors showed increased number of mitochondrial and nuclear DNA lesions in blood cells from FA patients compared with controls. A link between frataxin expression, DNA repair and tumor initiation was observed in murine liver (13). Analysis of diploid frataxin-deficient yeast also showed nuclear DNA damage, which was evidenced by higher levels of illegitimate mating, higher rate of spontaneous mutation and increased sensitivity to the DNA-alkylating methyl methanesulfonate (MMS) and to the replication inhibitor hydroxyurea than controls (14). Furthermore, deletion of the glutathione peroxidase encoding gene *GPX1* in frataxin-deficient cells resulted in a marked increase in the nuclear mutation rate. These results led the authors to suggest that the increased spontaneous nuclear damage in Δ*yfh1* cells was caused by H_2O_2 generated in the mitochondria (14). In line with this hypothesis, Δ*yfh1* cells are extremely sensitive to H_2O_2 treatment (21). In addition, different studies in yeast, *Drosophila* and patient fibroblasts showed that H_2O_2 levels increase in frataxin-deficient cells (22–24).

ROS can induce several types of lesions in DNA, such as oxidized bases, apurinic/apyrimidinic (AP) sites, base deamination products, oxidized sugar fragments and DNA-strand breaks. The four DNA bases can be directly oxidized by ROS. The major products of oxidation of purines are 8-oxo-7,8-dihydro-2′-deoxyguanosine (8-oxodG) and 2, 6-diamino-4-hydroxy-5-formamidopyrimidine (FapydG) for guanine and 8-oxodA and FapydA for adenine. Oxidation of cytidine results mainly in the 5-hydroxy-2′-deoxycytidine (OH5dC) and oxidation of thymidine results in thymine glycol. These and other damaged bases, if not repaired, may have miscoding properties and lead to mutation upon replication or block progression of the replication fork (11,25). The vast majority of damaged and mispaired DNA bases, resulting not only from oxidation but also from alkylation or X-ray exposition, are repaired by the base excision repair (BER) pathway in yeast and mammalian cells (12,26). The BER pathway is initiated by the recognition and removal of the damaged or inappropriate bases by bifunctional *N*-glycosylases/AP-lyases (three enzymes in yeast, Ogg1, Ntg1 and Ntg2), creating an AP site. This abasic site is then repaired by the AP endonucleases, Apn1 and Apn2, or by AP lyases (25,26). In addition, the nucleotide excision repair (NER) pathway can be used to repair AP sites when the BER pathway is deficient (26). Ntg1 and Ntg2 are closely related and, as opposed to Ogg1, exhibit a broad substrate specificity catalyzing the removal of oxidized pyrimidines and purines (26,27). Ntg1 is localized to the nucleus or to the mitochondria in response to oxidative DNA damage, whereas Ntg2 is exclusively nuclear and has an iron–sulfur cluster (27–29). Single deletion of the *NTG1* and *NTG2* genes causes increased spontaneous and H_2O_2-induced mutagenesis compared with the wild-type (27). Apn1 is the major AP endonuclease in the cell accounting for >97% of the AP-endonuclease/3′-diesterase activity in wild-type cells (30). It is localized in the nucleus and in the mitochondria through physical interaction with Pir1 (31). Apn1-deficient cells show increased spontaneous nuclear and mitochondrial mutation frequencies (32).

Oxygen exposition causes the emergence of the two main deleterious phenotypes observed in the yeast Δ*yfh1* mutant; iron–sulfur cluster deficiency and oxidative stress. Transition from anaerobiosis to aerobiosis leads to degradation of the aconitase iron–sulfur cluster and a decrease of its activity, accumulation of cytosolic and mitochondrial carbonylated proteins and inhibition of the proteasome activity in Δ*yfh1* cells (33). Here, we report that transition from anaerobiosis to aerobiosis of Δ*yfh1* cells causes down-regulation of antioxidant defenses and that the increase in the amounts of ROS induces mitochondrial and nuclear DNA damage. In addition, we show that the Apn1 AP-endonuclease is essential for the repair of oxidatively modified DNA bases in Δ*yfh1* cells.

RESULTS

Antioxidant defenses in Δ*yfh1* cells are down-regulated in aerobiosis but not in anaerobiosis

Previous data showed that the anaerobiosis to aerobiosis transition is an inducer of oxidative stress in Δ*yfh1* cells (33). In addition, transcription of several genes encoding critical antioxidant enzymes (superoxide dismutase *SOD2*; catalases *CTT1* and *CTA1*; thiol peroxidase *HYR1*; glutaredoxins *GRX4* and *GRX5*; thioredoxin *TRX1* and thioredoxin reductase *TRR1*) were significantly repressed in Δ*yfh1* compared with wild-type cells in aerobiosis (21). Real-time quantitative PCR (RT-qPCR) was therefore used to investigate the expression of 22 genes implicated in the oxidative stress response in cells cultivated under strict anaerobiosis (2 ppm O_2) and aerobiosis (Table 1). In anaerobiosis, the expression of most genes in Δ*yfh1* was similar to the wild-type or induced (*AHP1*, *GTT2* and *TRX3*). However, expression of the *GRX4*, *GRX5* and *TRR1* genes, which were repressed in aerobiosis, was also moderately repressed (1.2–1.5-fold) under anaerobiosis in Δ*yfh1* cells. In aerobiosis, only one gene was induced in Δ*yfh1* cells (*GTT2*), while nine genes were repressed. The expression profile of the 11 genes that were either induced or repressed in anaerobiosis or aerobiosis was determined during transition from anaerobiosis to aerobiosis (Table 1 and Fig. 1A). All genes were repressed 30–60 min after oxygen exposition in Δ*yfh1* cells. For *SOD2*, *CTT1*, *CTA1*, *AHP1*, *GRX4*, *GRX5* and *TRR1* genes repression occurred 15 or 30 min after transition, which persisted under aerobiosis. The expression of *GTT3* and *TRX2* increased 15 min after transition to aerobiosis but declined after 30 min. These findings show that frataxin deficiency in yeast cells leads to deregulation of the transcription of several genes that encode enzymes central to protection against oxidative damage in aerobic conditions.

Glutathione is a main protective antioxidant in yeast cells. We have shown that the glutathione levels of the Δ*yfh1*

Table 1. Expression of genes implicated in the antioxidant defense and in the BER pathway in Δyfh1 cells

Gene	Δ*yfh1*/ WT ratio (mean ± SE)				
	Anaerobiosis	15 min	30 min	60 min	Aerobiosis
SOD1, Cu,Zn superoxide dismutase	1.10 ± 0.03				0.79 ± 0.02
SOD2, Mn superoxide dismutase	1.32 ± 0.08	0.58 ± 0.02	0.31 ± 0.08	0.63 ± 0.04	0.44 ± 0.02
CTT1, catalase T	1.11 ± 0.07	1.23 ± 0.04	0.40 ± 0.06	0.38 ± 0.01	0.20 ± 0.02
CTA1, catalase A	1.70 ± 0.09	0.41 ± 0.05	0.35 ± 0.07	0.43 ± 0.04	0.50 ± 0.03
AHP1, peroxiredoxin	2.72 ± 0.21	0.89 ± 0.12	0.36 ± 0.09	0.30 ± 0.02	0.64 ± 0.02
GSH1, gamma-glutamylcysteine synthetase	1.24 ± 0.03				0.90 ± 0.04
GPX1, glutathione peroxidase	1.89 ± 0.06				0.96 ± 0.09
GPX2, glutathione peroxidase	1.21 ± 0.03				1.17 ± 0.07
HYR1, thiol peroxidase	0.97 ± 0.03				0.56 ± 0.02
GTT1, glutathione transferase	1.20 ± 0.09				1.40 ± 0.12
GTT2, glutathione transferase	2.08 ± 0.24	0.92 ± 0.17	0.53 ± 0.07	0.60 ± 0.09	3.09 ± 0.84
GTT3, glutathione transferase	1.20 ± 0.08	3.19 ± 0.89	1.95 ± 0.76	0.46 ± 0.08	0.24 ± 0.02
GRX1, glutaredoxin	1.62 ± 0.06				1.76 ± 0.13
GRX2, glutaredoxin	1.02 ± 0.04				0.73 ± 0.04
GRX3, glutaredoxin	1.29 ± 0.02				0.85 ± 0.04
GRX4, glutaredoxin	0.65 ± 0.01	1.07 ± 0.13	0.44 ± 0.02	0.09 ± 0.01	0.16 ± 0.01
GRX5, glutaredoxin	0.82 ± 0.03	0.91 ± 0.06	0.46 ± 0.05	0.37 ± 0.02	0.33 ± 0.02
TRX1, thioredoxin	0.94 ± 0.05	1.59 ± 0.29	0.54 ± 0.09	0.64 ± 0.08	0.36 ± 0.02
TRX2, thioredoxin	1.08 ± 0.03				0.82 ± 0.04
TRX3, thioredoxin	2.11 ± 0.06	1.10 ± 0.18	0.38 ± 0.05	0.57 ± 0.02	1.21 ± 0.09
TRR1, thioredoxin reductase	0.77 ± 0.02	0.68 ± 0.08	0.15 ± 0.04	0.42 ± 0.07	0.51 ± 0.02
TRR2, thioredoxin reductase	1.32 ± 0.03				0.74 ± 0.02
APN1, AP-endonuclease	1.48 ± 0.15	0.99 ± 0.09	0.38 ± 0.05	0.35 ± 0.09	1.02 ± 0.18
NTG1, *N*-glycosylase/AP-lyase	0.91 ± 0.09	0.73 ± 0.08	0.28 ± 0.06	0.36 ± 0.07	0.82 ± 0.15
NTG2, *N*-glycosylase/AP-lyase	1.26 ± 0.12	1.08 ± 0.11	0.33 ± 0.04	0.49 ± 0.03	1.28 ± 0.08
FET3, ferroxidase	17.55 ± 2.99				50.25 ± 4.39

The *FET3* gene was included as a control.

mutant are disturbed compared with the wild-type in aerobic conditions (21,34). Interestingly, under anaerobiosis, the total glutathione levels in Δ*yfh1* and wild-type cells were significantly different but in the same range (1.2-fold difference, $P < 0.01$; 78.9 ± 2.1 nmoles glutathione/mg protein in Δ*yfh1* cells compared with 93.1 ± 3.8 nmoles glutathione/mg protein in wild-type cells; Fig. 1B). As observed previously, in aerobic conditions the total glutathione specific content was 2-fold decreased in Δ*yfh1* compared with wild-type cells (115.0 ± 8.6 nmoles glutathione/mg protein in Δ*yfh1* cells compared with 206.7 ± 23.5 nmoles glutathione/mg protein in wild-type cells). Time course experiments showed that the total glutathione levels of wild-type cells increased progressively from 10 to 30 min after transition to aerobiosis to attain values 2-fold higher than those observed in aerobically cultivated cells (Fig. 1C). Compared with wild-type cells, the response of Δ*yfh1* cells is more rapid but transient. A 3-fold increase in total glutathione content is observed 10 min after transition to aerobiosis and a return to basal level after 15 min (Fig. 1C). This shows that in wild-type cells, glutathione levels increase with the transition from anaerobiosis to aerobiosis, but in Δ*yfh1* cells this response to oxygen does not occur and could result in less protection against oxidative damage.

Transition from anaerobiosis to aerobiosis leads to increased ROS-mediated DNA-strand breaks in Δ*yfh1*

Since the cellular antioxidant defenses appear to be deregulated in Δ*yfh1* cells, increase in ROS accumulation was tested during the transition from anaerobiosis to aerobiosis using the fluorescent dye dihydroethidium (DHE). After exposure to oxygen, Δ*yfh1* cells showed significantly more ROS-driven DHE to ethidium conversion than wild-type cells at all time points investigated, as estimated by flow cytometry analysis (Fig. 2A). ROS accumulation in Δ*yfh1* cells peaked at 30 min (median DHE fluorescence at 30 min was 13.1 ± 0.8 in Δ*yfh1* cells and 7.9 ± 0.9 in wild-type cells, $P < 0.001$) and then decreased at 60 min. This decline in the ROS level is certainly transitory because in aerobic conditions, Δ*yfh1* mutant cells show higher ROS levels than wild-type cells (Fig. 2A).

We tested if cells accumulating ROS failed to adapt to oxygen conditions and died. ROS production is a key event in the induction of apoptosis in yeast cells. In addition, treatment of wild-type and Δ*yfh1* cells with low doses of H_2O_2 induces apoptosis (21,35). To test this possibility, cell death and apoptosis were monitored using the clonogenic test and TUNEL staining after transition from anaerobiosis to aerobiosis. No decrease in viability was observed in wild-type and Δ*yfh1* cells (data not shown), suggesting that cell death was not induced in these conditions. However, when formaldehyde fixed cells were tested for DNA-strand breaks by TUNEL assay, a significantly high level of positive cells was observed in Δ*yfh1* cells in aerobiosis. In anaerobiosis, <10% of the cells were positively stained for TUNEL in both wild-type and Δ*yfh1* strains (Fig. 2B). Significantly ($P < 0.01$), fewer Δ*yfh1* cells were stained after 60 min than 15 min of oxygen exposition. However, a high proportion of Δ*yfh1* cells from aerobic cultures were positively stained for TUNEL (60.2 ± 2.0% for Δ*yfh1* compared with 15.5 ± 0.2% for wild-type), consistent with the findings for ROS staining

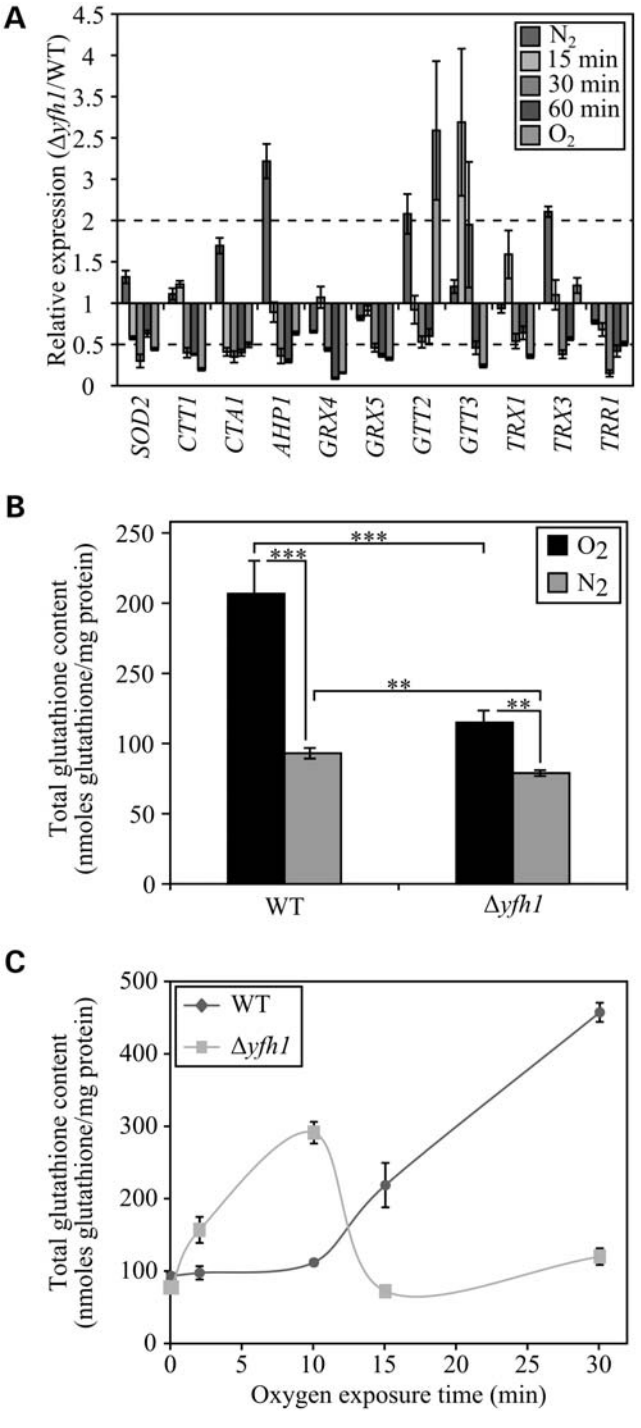

Figure 1. Antioxidant defenses in Δ*yfh1* cells during transition from anaerobiosis to aerobiosis. (**A**) Relative expression of genes implicated in the response to oxidative stress in Δ*yfh1* and wild-type cells. Data were obtained by RT-qPCR and represent means of the ratio Δ*yfh1*/WT ± SE from three (wild-type) or four (Δ*yfh1*) biological replicates. (**B**) Total glutathione levels in Δ*yfh1* and wild-type cells were determined using the enzymatic recycling assay and normalized to the protein content in exponentially growing cells in defined glucose medium. All data represent means ± SE for $n = 5$ cultures; $^{**}P < 0.01$, $^{***}P < 0.001$. (**C**) Total glutathione levels during transition from anaerobiosis to aerobiosis. All data represent means ± SE for $n = 4$ cultures.

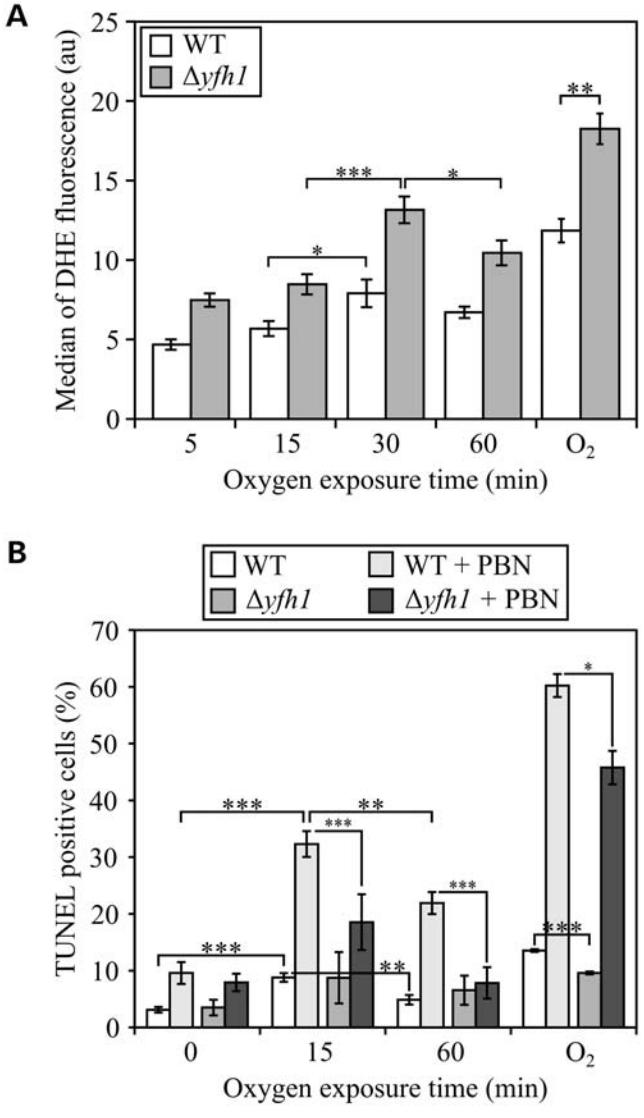

Figure 2. Transition of Δ*yfh1* cells from anaerobiosis to aerobiosis causes ROS accumulation and an increase in TUNEL staining. (**A**) ROS levels during transition from anaerobiosis to aerobiosis, and in aerobiosis, were evaluated using DHE staining under anaerobic conditions and fluorescence was quantified by flow cytometry. Data represent medians of fluorescence ± SE for $n = 16$ (transition) or $n = 3$ (aerobiosis) cultures; $^{*}P < 0.05$, $^{**}P < 0.01$, $^{***}P < 0.001$. Differences between Δ*yfh1* and wild-type strains are significant at all time points, $P < 0.001$. (**B**) Nuclear DNA-strand breaks were assayed by TUNEL staining and flow cytometry analysis. Treatment with 5 mM PBN significantly reduces the number of Δ*yfh1* cells positive for TUNEL staining. Data represent percentages of cells stained ± SE for $13 < n < 17$ cultures; $^{*}P < 0.05$, $^{**}P < 0.01$, $^{***}P < 0.001$. Legend: au, arbitrary units.

(Fig. 2A). The effect of the spin trap phenyl *N*-tert-butylnitrone (PBN) was tested. Treatment with 5 mM PBN reduced TUNEL staining of Δ*yfh1* cells close to wild-type levels during transition from anaerobiosis to aerobiosis and in aerobiosis (Fig. 2B), indicating that oxygen exposition caused an increase in ROS production and in DNA-strand breaks.

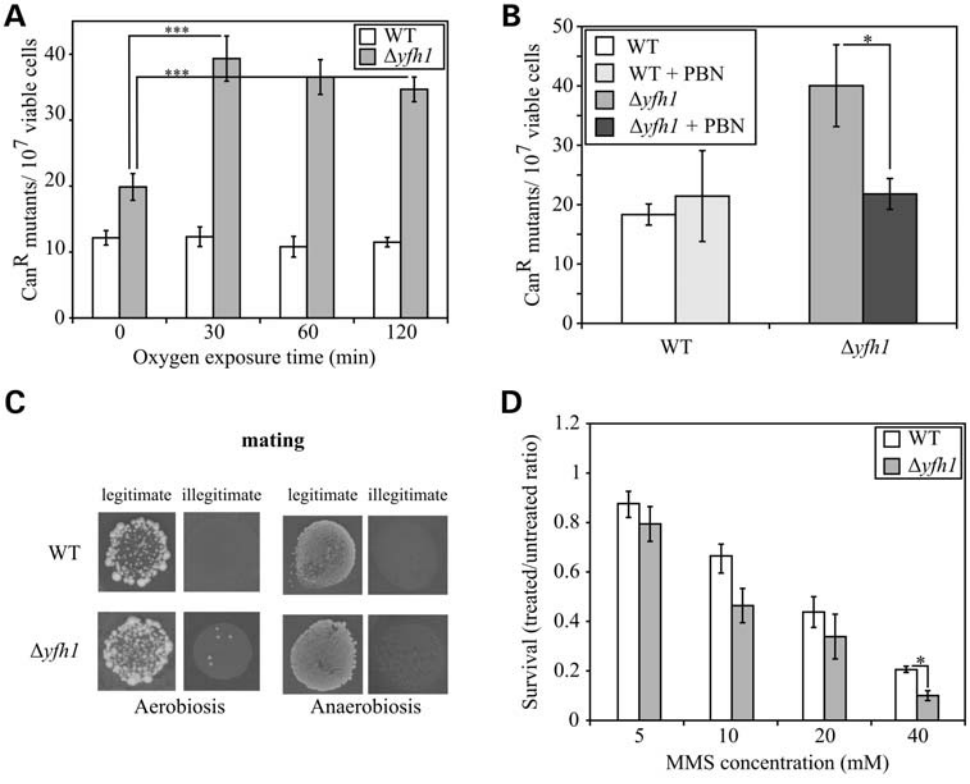

Figure 3. Transition of Δ*yfh1* cells from anaerobiosis to aerobiosis causes DNA damage. (**A**) Can^R spontaneous mutant frequencies determined during transition from anaerobiosis to aerobiosis of exponentially growing cultures on the SDTe medium. Data represent means ± SE for $n = 5$ cultures. The difference between mutation frequency in anaerobiosis and all times in aerobiosis in Δ*yfh1* cells is highly significant, $P < 0.001$. (**B**) Can^R spontaneous mutant frequencies determined in aerobic stationary cultures in the presence and absence of PBN. Data represent means ± SE for $4 < n < 5$ cultures; $^*P < 0.05$. (**C**) Illegitimate mating increases in aerobic conditions in Δ*yfh1* cells. Crosses of *Mat*α wild-type and Δ*yfh1* cells with *Mat*a tester strain (legitimate) or with *Mat*α (illegitimate) tester strain in anaerobiosis and aerobiosis are shown. (**D**) The survival ratio of exponentially growing cells in SD medium to 30 min MMS treatment in aerobiosis. Data represent ratio of means ± SE for $n = 3$ cultures; $^*P < 0.05$.

Δ*yfh1* cells show increased oxygen-dependent nuclear and mitochondrial DNA damage

The preceding results suggested that increased nuclear DNA lesions occurred when Δ*yfh1* cells were exposed to oxygen. Since DNA damage was previously reported in diploid Δ*yfh1*/Δ*yfh1* cells in aerobiosis (14), the spontaneous mutation rate at the *CAN1* locus was determined by canavanine resistance in anaerobiosis and aerobiosis. The results showed that haploid Δ*yfh1* cells have a 2-fold increased Can^R mutation frequency compared with the wild-type in aerobiosis and in anaerobiosis (Fig. 3A and B). In addition, both wild-type and Δ*yfh1* strains showed increased mutation frequencies in aerobiosis compared with anaerobiosis. Transition from anaerobiosis to aerobiosis did not cause a significant change in the Can^R mutation frequency in wild-type cells (Fig. 3A). However, in Δ*yfh1*, a rapid increase in the mutation frequency was observed 30 min after transition to aerobiosis (Fig. 3A), in agreement with the increase in ROS levels and DNA-strand breaks observed. Moreover, addition of PBN to aerobic cultures led to a reduction in the mutation frequency in Δ*yfh1* cells to values similar to that obtained in wild-type cells (with PBN, 21.4 ± 7.6 Can^R mutants/10^7 viable cells in wild-type and 26.3 ± 4.9 Can^R mutants/10^7 viable cells in Δ*yfh1* cells; without PBN, 18.3 ± 1.7 Can^R mutants/10^7 viable cells in wild-type and 40.0 ± 6.9 Can^R mutants/10^7 viable cells in Δ*yfh1* cells) (Fig. 3B). Together, these data show that oxygen exposure and ROS accumulation cause oxidative nuclear DNA lesions in Δ*yfh1* cells.

Other indicators of nuclear DNA damage were tested. Double-strand breaks in DNA arise mainly during replication and require homologous recombination for repair (36). Illegitimate mating of *Mat*α cells can occur via point mutations in the locus converting it to *Mat*a or inactivating it, or by chromosome III recombination events between *Mat*α and *HMR*a loci. Thus, illegitimate mating can be used as an indirect measure of recombination and double-strand break repair. The frequency of mating of *Mat*α wild-type and Δ*yfh1* cells with a *Mat*α tester strain was identical and close to 0 in anaerobiosis; however, it was moderately increased in aerobiosis in Δ*yfh1* compared with wild-type cells (2.6 ± 0.8 colonies/10^8 Δ*yfh1* cells and 0 colonies with wild-type cells, $n = 16$; Fig. 3C). In addition, the Δ*yfh1* cells were not sensitive to hydroxyurea (up to 100 mM; data not shown), which inhibits replication and causes double-strand breaks in the DNA. Sensitivity to the base-alkylating MMS was also determined. Although the mutant was more sensitive than the wild-type, the difference between the survival of Δ*yfh1* and wild-type cells was only statistically significant when treated with 40 mM MMS (Fig. 3D). These data suggest that double-strand

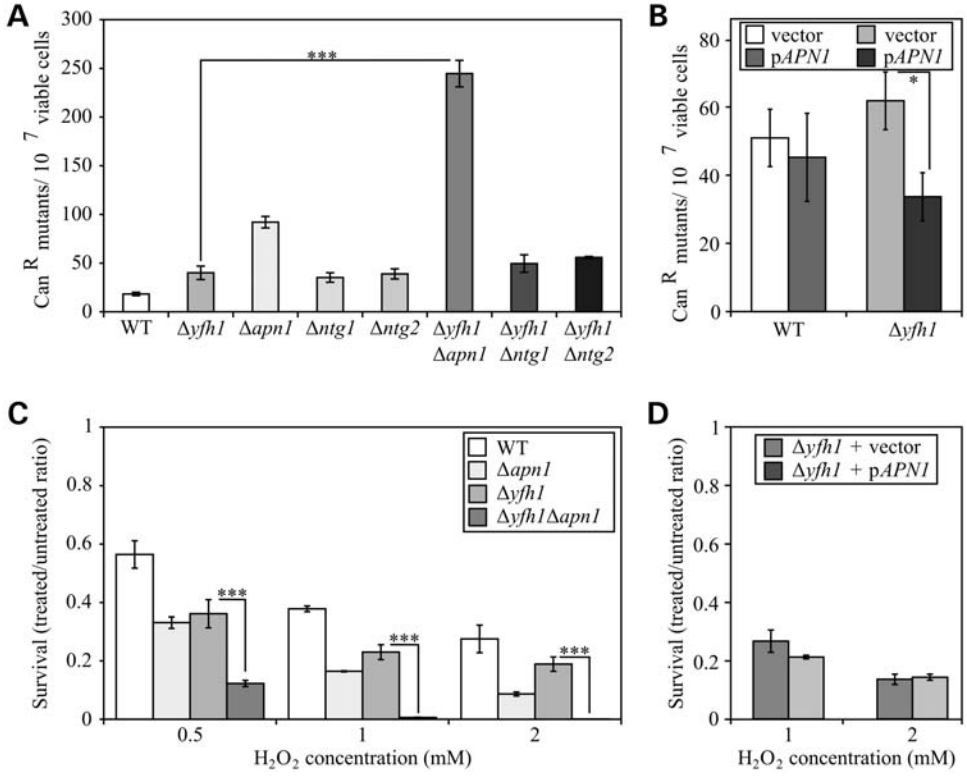

Figure 4. Apn1, but not Ntg1 or Ntg2, is necessary for repair of damaged bases in Δ*yfh1* cells. (**A**) Can^R spontaneous mutant frequencies determined in aerobic stationary cultures. Data represent means ± SE for $5 < n < 10$ cultures; $^{***}P < 0.001$. (**B**) Can^R spontaneous mutant frequencies in aerobic stationary cultures of wild-type and Δ*yfh1* cells carrying the vector p426GPD1 or a construct that overexpresses *APN1*. Data represent means ± SE for $n = 5$ cultures; $^{*}P = 0.07$. (**C** and **D**) The survival ratio of exponentially growing cells in SD medium to 30 min H_2O_2 treatment in aerobiosis. Data represent ratio of means ± SE for $n = 3$ cultures; $^{***}P < 0.001$.

breaks are a minor type of lesion in the genomic DNA of Δ*yfh1* cells.

Loss of mitochondrial DNA (rho$^-$ and rho$^\circ$ cells) is a characteristic phenotype of frataxin deficiency in yeast cells (17–19). To detect complete or partial loss of mitochondrial DNA, colonies resulting from crosses with the *Mat*a ρ^0 tester strain were performed in anaerobiosis and aerobiosis and diploid colonies were tested for growth in the medium containing glycerol as the only carbon source. In anaerobiosis, no loss of mitochondrial DNA was observed (400 colonies analyzed) compared with only 1.2% of cells that retain mitochondrial DNA in aerobiosis (900 colonies analyzed). Therefore, mitochondrial DNA loss is oxygen exposition dependent. Loss of mitochondrial DNA mediates mutagenesis of the nuclear genome (37); however, it cannot explain the increased mutation frequency in Δ*yfh1* cells because 6–8 h (two generations) after transition from anaerobiosis to aerobiosis, no glycerol-negative colonies were observed (400 colonies analyzed).

Apn1 is necessary for repair of modified DNA bases in Δ*yfh1* cells

Given that Δ*yfh1* cells accumulate oxidative DNA lesions, we investigated whether the BER pathway was defective in these cells. To this end, the function of Ntg1, Ntg2 and Apn1 was investigated. Although the expression of these genes in anaerobiosis and aerobiosis was not altered in Δ*yfh1* compared with wild-type cells, they were repressed after 30 min of oxygen exposition (Table 1). We examined the phenotypes of the double deletions Δ*yfh1*Δ*ntg1*, Δ*yfh1*Δ*ntg2* and Δ*yfh1*-Δ*apn1* and overexpression of the *NTG1* and *APN1* genes in wild-type and Δ*yfh1* cells. The Δ*yfh1*Δ*apn1* strain, but not the Δ*yfh1*Δ*ntg1* and Δ*yfh1*Δ*ntg2* strains, presented a growth defect in liquid and solid media compared with the Δ*yfh1* cells (data not shown; see below). Deletion of *APN1* in Δ*yfh1* cells resulted in an important increase in the spontaneous Can^R mutagenesis (Fig. 4A, Table 1). On the contrary, deletion of the *NTG1* and *NTG2* genes in Δ*yfh1* cells caused only a small, non-significant, increase in the spontaneous mutation frequencies (Fig. 4A). In agreement with this, Δ*yfh1* cells overexpressing the *APN1* gene showed a 2-fold decrease in mutation frequencies compared with cells harboring the vector (Fig. 4B). As for deletion, overexpression of the *NTG1* gene did not cause any change in Δ*yfh1* cells (data not shown). Since the Δ*yfh1* strain is highly sensitive to H_2O_2, all mutants were treated 30 min with 0.5 to 2 mM H_2O_2 and the surviving fraction of the population determined. The Δ*yfh1*Δ*apn1* mutant was extremely sensitive to H_2O_2 (Fig. 4C), but not the Δ*yfh1*Δ*ntg1* and Δ*yfh1*Δ*ntg2* double mutants (data not shown). In contrast, overexpression of *APN1* in Δ*yfh1* cells did not lead to an increase in resistance to H_2O_2 (Fig. 4C). Taken together, these data suggest that Apn1 AP-endonuclease is a central enzyme in the repair of damaged bases in Δ*yfh1* cells.

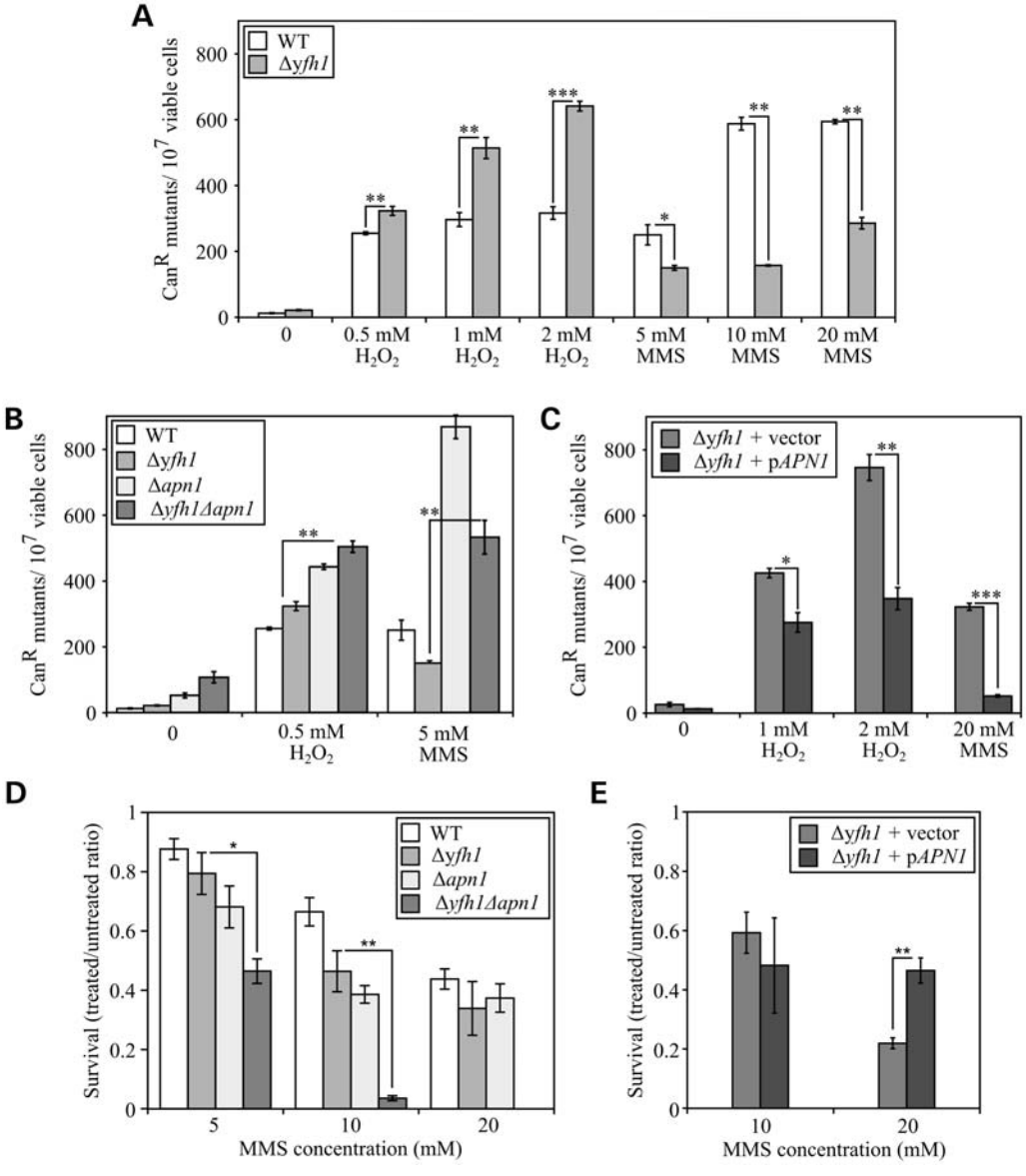

Figure 5. H_2O_2- and MMS-induced mutagenesis and survival. (**A**–**C**) Can^R spontaneous mutant frequencies were determined in exponentially growing cells treated for 30 min with different H_2O_2 and MMS concentrations. Data represent means ± SE for $3 < n < 5$ cultures; $^*P < 0.05$; $^{**}P < 0.01$; $^{***}P < 0.001$. (**D** and **E**) The survival ratio of exponentially growing cells to MMS treatment for 30 min. Data represent ratio of means ± SE for $n = 3$ cultures; $^*P < 0.05$; $^{**}P < 0.01$.

Mutagenesis in Δ*yfh1* cells exposed to oxidizing and alkylating chemicals

Exposure of yeast cells to H_2O_2 and MMS causes oxidation and alkylation of DNA bases, respectively, resulting in increased mutagenesis. The data presented here show oxidative damage to DNA in Δ*yfh1* cells but no noticeable sensitivity to MMS. Therefore, we investigated the effect of H_2O_2 and MMS on the mutation frequency in frataxin-deficient mutants. Exposure of Δ*yfh1* cells to rising H_2O_2 concentrations led to a marked increase in Can^R mutation frequencies, while in wild-type cells the increase was small between 0.5 and 2 mM H_2O_2 (Fig. 5A). The double Δ*yfh1*Δ*apn1* mutant showed higher mutation frequency to 0.5 mM H_2O_2 (higher concentrations were difficult to test because the survival of Δ*yfh1*Δ*apn1* cells treated with H_2O_2 was very low) than Δ*yfh1* and Δ*apn1* cells (Fig. 5B). Accordingly, overexpression of the *APN1* gene in Δ*yfh1* reduced the mutation frequency after H_2O_2 treatment (Fig. 5C). In addition, the fact that mutation frequencies in Δ*apn1* are higher than those observed in Δ*yfh1* cells argues in favor of the essential role of Apn1 in the repair of oxidized bases in Δ*yfh1*.

The results obtained after treatment of Δ*yfh1* cells with MMS were unexpected. Although exposure of Δ*yfh1* cells to MMS caused an increase in Can^R mutation frequencies compared with untreated conditions, the levels were 1.6 to 3.7 times lower than those observed for wild-type cells (Fig. 5A). The Δ*yfh1*Δ*apn1* mutation frequencies were

intermediate between Δ*yfh1* and Δ*apn1*, again pointing to a resistance of frataxin-deficient cells to MMS-induced mutagenesis (Fig. 5B). However, the mutant Δ*yfh1*Δ*apn1* was very sensitive to MMS, with <0.5% survival with a 20 mM treatment for 30 min (Fig. 5D). Overexpression of *APN1* in Δ*yfh1* cells increased cell survival and reduced by more than 6-fold the mutation frequency in response to MMS treatment (Fig. 5C and E). In contrast, when Δ*yfh1* cells were exposed to H_2O_2, the overexpression of *APN1* did not change cell survival (Fig. 4D) and only reduced mutagenesis by a factor of 2.5 (Fig. 5C).

Transition from anaerobiosis to aerobiosis leads to cell cycle arrest in Δ*yfh1* cells

Cells respond to DNA damage and defects in chromosome replication by delaying cell cycle that allows time for DNA repair to occur. Checkpoints are signaling pathways that identify damage and arrest cell cycle. In *S. cerevisiae*, DNA damage checkpoints delay the G1/S transition, slow replication (S-phase) and block G2/M transition of the cell cycle (38). Therefore, we tested the impact of oxidative DNA damage on the cell cycle in Δ*yfh1* cells shifted from anaerobiosis to aerobiosis. To follow cell cycle progression in an asynchronous cell population, we chose to use multispectral imaging flow cytometry because it allows the analysis of DNA content and morphological markers of cell cycle progression in a large number of cells (39,40). The analysis of the data is based on the following criteria: cells in G1 have 1n DNA content, single round nuclei and present no buds; the DNA content of cells in S-phase progressively increase from 1n to 2n, cells have emergent buds and undivided nuclei; G2/M is characterized by 2n DNA content and divided nuclei. The DNA content is determined by the intensity of the SYTOX Green stain and the nuclear morphology by the aspect ratio (ratio of width to length) of the DNA stain. In a scatter plot showing these two features, the three populations of cells can be clearly identified as shown in Figure 6A.

In aerobiosis, no significant difference in the cell cycle was observed between wild-type and exponentially growing Δ*yfh1* cells, although the number of cells in G1 was slightly higher in the mutant (Fig. 6B). No difference was observed between the two strains in anaerobiosis either. The percentage of cells in G1-phase was increased in anaerobiosis compared with aerobiosis (Fig. 6B), in agreement with the slower growth rate of the wild-type and Δ*yfh1* in anaerobiosis (data not shown). Transition from anaerobiosis to aerobiosis induced a temporary cell cycle arrest in Δ*yfh1* but not in wild-type cells. After 30 min of oxygen exposition, a significant ($P < 0.01$) increase in the number of cells in G1 and a decrease in the number of cells in G2/M were visible (Fig. 6B). Two hours later cell cycle resumed. These data show that exposition of Δ*yfh1* cells to oxygen causes cell cycle arrest at G1 and delays replication. The single Δ*apn1* mutant showed no perturbation in cell cycle when the cells were exposed to oxygen (Fig. 7A). The growth of the double Δ*yfh1*Δ*apn1* mutant was defective in anaerobiosis and aerobiosis, which was perceptible in the distribution of cells in G1 (almost 50%) and G2/M (less than 20%) populations (Fig. 7A). Exposition of these cells to oxygen block cells in G1- and S-phases (1n DNA content). On the contrary, the overexpression of *APN1* rescues the cell cycle arrest phenotype in Δ*yfh1* cells (Fig. 7B). These data further establish the role of Apn1 in the repair of oxidized bases in Δ*yfh1* cells.

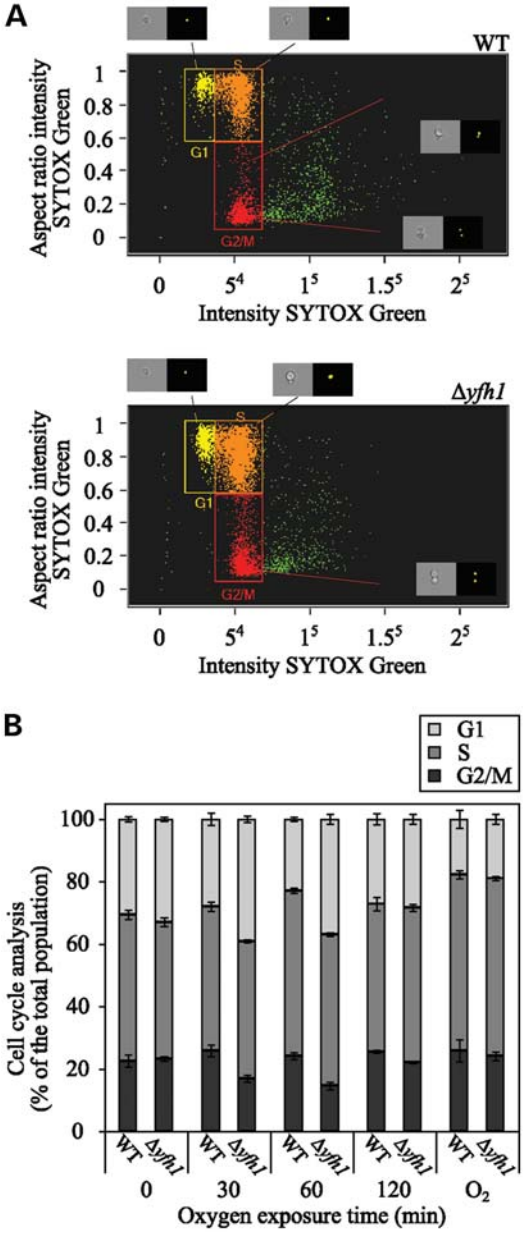

Figure 6. Cell cycle analysis in the wild-type and Δ*yfh1* using multispectral imaging flow cytometry. (**A**) A scatter plot of the aspect ratio and fluorescence intensity of SYTOX Green allows the identification of the G1, S and G2/M cell populations; in this case in aerobic asynchronous wild-type and Δ*yfh1* cultures. Brightfield and SYTOX Green images from the three regions are shown. (**B**) Transition of Δ*yfh1* cells from anaerobiosis to aerobiosis causes cell cycle delay. The quantification of cells in G1, S and G2/M populations was done from scatter plots as shown in (A). Data represent means ± SE for $n = 3$ cultures. Differences in G1 and G2/M data of Δ*yfh1* cultures comparing anaerobiosis and all times of oxygen exposition are statistically significant ($P \leq 0.05$).

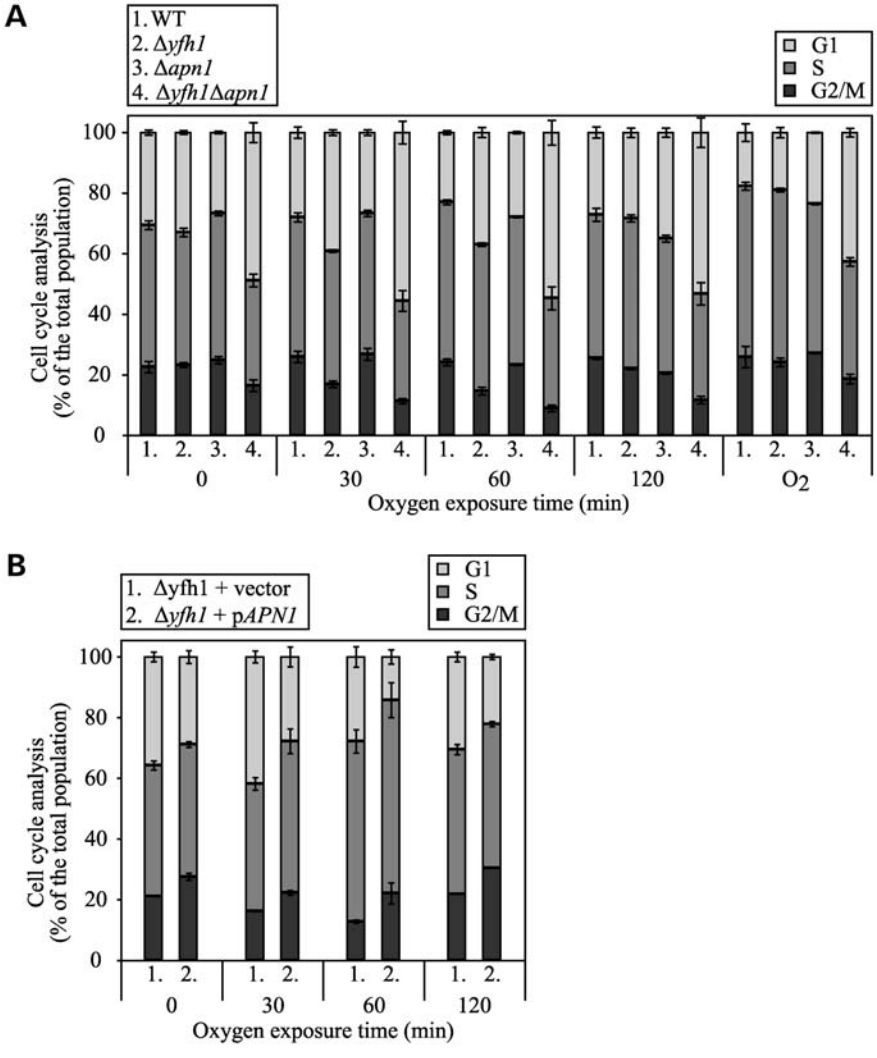

Figure 7. Effect of Apn1 in cell cycle delay in Δ*yfh1* cells. (**A** and **B**) The quantification of cells in the G1, S and G2/M populations was done from scatter plots. Data represent means ± SE for $3 < n < 4$ cultures. Differences in G1, S and G2/M data between Δ*yfh1* and Δ*yfh1*Δ*apn1* cultures are statistically significant at all times of oxygen exposition ($P \leq 0.05$). Differences in G1 and G2/M data between Δ*yfh1* strains overexpressing or not *APN1* are statistically significant at all times of oxygen exposition ($P \leq 0.05$).

DISCUSSION

Oxidative genome damage has been implicated in the etiology of several neurological disorders. Here, we present evidence that one of the pleiotropic effects of increased ROS and oxidative stress in frataxin-deficient yeast cells is oxidation of DNA bases and requirement of Apn1 of the BER pathway for repair and cell survival.

Previous observations showed that exposition of yeast frataxin-deficient cells to oxygen for 16 h caused oxidative stress and loss of activity of aconitase, an iron–sulfur cluster enzyme (33). Although in anaerobiosis no defect is observed in antioxidant defense, in aerobiosis several genes encoding important antioxidant enzymes are repressed, glutathione levels are low and ROS levels are high (21,34). The effect of oxygen in anaerobically grown Δ*yfh1* cells is very rapid. The first response to oxygen exposition is the increase in total glutathione content after 10 min. At 15 min, glutathione levels decrease, several antioxidant genes are repressed and DNA-strand breaks can be detected by the TUNEL assay. At 30 min, cell cycle is arrested at G1/S and mutation frequency is increased. Two hours later, cell cycle is reinitiated despite the oxidative stress state and high spontaneous mutation frequency in Δ*yfh1* cells. Therefore, exposition of Δ*yfh1* cells to oxygen causes an oxidative burst in the first 15 min due to inefficient antioxidant defense and adaptation to aerobiosis after 60–120 min. Mitochondrial iron–sulfur cluster biosynthesis and integrity of mitochondrial DNA are important factors for the maintenance of nuclear genome stability (37,41,42). Loss of mitochondrial DNA in yeast leads to cell cycle arrest at G1 and progressive loss of viability. However, the cells reentering the cell cycle exhibit increased genome instability and selection for nuclear mutations that improve growth in the absence of mitochondrial DNA (41). This process is mediated by the reduction in the inner mitochondrial membrane electrochemical potential, increase in

oxidative damage and impaired mitochondrial and nuclear/cytosolic Fe–S cluster assembly (41). It is possible that a similar process of adaptation occurs when Δ*yfh1* cells are exposed to oxygen for the first time, although the chronology of the events is not the same. Increase in nuclear genome instability takes place before mitochondrial DNA loss, and this could be due to the low iron–sulfur cluster biosynthesis in Δ*yfh1* cells. Upon oxygen exposition, oxidative damage to DNA causes cell cycle delay and selection for mutations that improve survival of Δ*yfh1* cells. In agreement with this hypothesis, accumulation of spontaneous suppressor mutations at a high frequency has been described in Δ*yfh1* (43). Independent analysis of several spontaneous mutants identified a single amino acid substitution in the Isu1 scaffold protein that bypasses the need of frataxin for iron–sulfur cluster assembly (44).

In yeast, frataxin deficiency does not induce a general sensitivity to DNA-damaging agents (14). Here, we show that lesions in the DNA in Δ*yfh1* cells are mainly due to oxidative modifications of DNA bases and single-strand breaks. Accordingly, H_2O_2 treatment causes a considerable increase in mutation frequency. However, the reason why Δ*yfh1* cells are more resistant than wild-type cells to MMS-induced mutagenesis is not clear. Treatment of wild-type yeast cells growing on a glucose-rich medium with MMS triggers inhibition of respiration and glycolysis, enhanced ROS production and increased glucose flow through the pentose-phosphate pathway (45). The metabolism in Δ*yfh1* cells is considerably different from that observed in wild-type cells; in particular, the pentose-phosphate pathway is strongly stimulated (34), which could account for the resistance of Δ*yfh1* cells to MMS treatment.

Oxidative DNA damage is largely repaired by the BER pathway. The AP endonucleases and AP lyases act at the same step in the BER pathway but have different enzymatic activities (26). AP-endonucleases cleave DNA at the 5′-side of an AP site or of a modified base yielding single-strand breaks with a 5′-deoxyribosephosphate. AP lyases excise oxidized bases by cleavage of the phosphodiester backbone on the 3′-side yielding single-strand breaks with a 3′-α,β-unsaturetedaldehydic end. Apn1 is essential for the repair of oxidative lesions in the nuclear DNA of Δ*yfh1* cells. In the absence of Apn1, AP sites are mostly incised by Ntg1 and Ntg2, but Ogg1 and the NER pathway can serve as backup activities (26,27). It is possible that these *N*-glycosylases/AP lyases and the NER pathway are less active in Δ*yfh1* cells. Ntg2 and the helicase Rad3, a subunit of the RNA polymerase II initiation complex TFIIH, from the NER pathway are iron-cluster enzymes and expected to have decreased activities in Δ*yfh1* cells (26,46). However, Δ*yfh1*Δ*ntg1* and Δ*yfh1*Δ*ntg2* mutants do not show increased spontaneous mutagenesis. The double Δ*yfh1*Δ*apn1* mutant presents growth defects, high spontaneous and induced mutagenesis and is extremely sensitive to oxidant treatment. These phenotypes ascertain the deleterious effect of oxidative DNA damage and the importance of Apn1 for repair in frataxin-deficient yeast cells.

In mammalian cells, Ape1 is the functional homologous protein of yeast Apn1. Ape1 is a multifunctional protein; in addition to its AP endonuclease activity in the BER pathway, it is a redox-dependent activator of several stress-induced transcription factors, such as AP-1, NF-kB, HIFα and p53 (47). Although the AP endonuclease activity is conserved from bacteria to humans, the redox function is specific to mammals. The redox activity of Ape1 depends on several cysteine residues that are reduced by thioredoxin and maintain transcription factors in a reduced (active) state. Therefore, Ape1 is a master regulator of oxidative stress response in mammalian cells through regulation of gene transcription and repair of DNA, but also by its control of the intracellular redox state by inhibiting ROS production (48). Decrease in the Ape1 levels in primary rat hippocampal and sensory neuron cultures leads to oxidative DNA damage, increase in apoptosis and sensitivity to H_2O_2 (49). Although some reports exist on this aspect, DNA damage has been disregarded in the pathophysiology of FA. However, oxidation of DNA bases and repair could be important factors in the progression rate of the disease.

MATERIALS AND METHODS

Yeast strains and growth conditions

The *Saccharomyces cerevisiae* strains used in this study were derived from cycloheximide-resistant YPH499 (*MATa ura3-52 lys2-801(amber) ade2-101(ochre) trp1-Δ63 his3-Δ200 leu2-Δ1 cyh2*) and YPH500 (*MATα ura3-52 lys2-801(amber) ade2-101(ochre) trp1-Δ63 his3-Δ200 leu2-Δ1 cyh2*) strains, referred to here as 'wild-type', and the *yfh1* shuffle strain described previously (50). In the shuffle strain, the *yfh1* mutation is covered by pRS318-*YFH1*, a plasmid containing the CEN, *CYH2* and the *YFH1 Hin*dIII genomic fragment. To avoid the appearance of suppressor mutations and loss of mitochondrial DNA, the plasmid was removed regularly under anaerobic conditions by counter selection on medium containing 10 μg/ml cycloheximide, which is toxic in the presence of the *CYH2* allele. The resulting mutant was named Δyfh1 (*MATα ura3–52 lys2–801(amber) ade2-101(ochre) trp1-Δ63 his3-Δ200 leu2-Δ1 cyh2 Δyfh1*::*TRP1*).

The YPH500 (*MATα*) wild-type strain was used to construct strains deleted for the *NTG1*, *NTG2* and *APN1* genes and strains overexpressing the *NTG1* and *APN1* genes. For the construction of the Δ*ntg1*::*HIS3MX6*, Δ*ntg2*::*HIS3MX6* and Δ*apn1*::*HIS3MX6* strains, the coding regions were replaced by the *HIS3MX6* gene, which was amplified from plasmid pFA6a-HIS3MX6 by PCR using the primer sets: 5′-GCCACA CCATTGGACCCCTCGATCCTTGTCACTCCGGCCTCGG ATCCCCGGGTTAATTAA-3′ and 5′-CTGTTTTCTCCTCG TGTTTAACATTGATTTCCGCCTCCACGTGAATTCGAG CTCGTTTAAAC-3′ for the *NTG1* gene; 5′-CGAATCAAGG ACTTGTGATGATCCGAGAACTTGGGGACGGGGATCC CCGGGTTAATTAA-3′ and 5′-CTGGCCATGCAGATCAAT TGACCAAATCCAACCAAAACGGGAATTCGAGCTCGT TTAAAC-3′ for the *NTG2* gene and 5′-ATGCCTTCGACAC CTAGCTTTGTTAGATCTGCTGTCTCGAGGATCCCCGG GTTAATTAA-3′ and 5′-TTATTCTTTCTTAGTCTTCCTCTT CTTTGTCATTTGTGACGAATTCGAGCTCGTTTAAAC-3′ for the *APN1* gene as described previously (51). Successful integration was verified using external primers to the genomic region deleted using the primer sets: 5′-AGACTGAAACTG GGCCAGAA-3′ and 5′-ACATATTAACAACTAGGCCTG C-3′ for *NTG1*; 5′-TTGACTGGATCAAGGCACTG-3′ and

5′-TTTGTAACCGTGTCCAACCA-3′ for *NTG2* and 5′-GTA AATATAAGATGACAAACTC-3′ and 5′-TAATCTACAAA AATTGATTACG-3′ for *APN1*. The multicopy plasmid p426GPD was used as a vector for the overexpression of the *NTG1* and *APN1* genes (52). The coding sequences were amplified by PCR using 5′-CGGGATCCATGCAAAAGATCAG TAAATAC-3′ and 5′-CGGAATTCTTAGTCCTCTACTTTA ACAGA-3′ primers for the *NTG1* and 5′-CGGGATCCATGC CTTCGACACCTAGCTT-3′ and 5′-CGGAATTCTTATTCT TTCTTAGTCTTCCTCTTC-3′ primers for the *APN1*, which carry 5′ *Bam*HI and *Eco*RI restriction sites, respectively. The amplified fragment was digested with *Bam*HI and *Eco*RI and inserted into the p426GPD plasmid under the control of the constitutive glyceraldehyde-3-phosphate dehydrogenase promoter (52). Overexpression of these genes was monitored by RT-qPCR and a 20–50-fold increase in mRNA was detected in wild-type and Δ*yfh1* strains carrying *APN1/NTG1* overexpressing plasmids compared with strains carrying the p426GPD vector.

Unless otherwise stated, liquid cultures were grown at 30°C in synthetic defined media (SD; yeast nitrogen base, ammonium sulfate, 2% D-glucose) plus the required amino acids and 200 mg/l adenine. For growth under anaerobic conditions, the medium was supplemented with 30 mg/l of ergosterol and 2 ml/l of Tween 80 (Te). Cells were plated weekly on YPD (1% yeast extract, 2% Bacto peptone, 2% D-glucose and 2.5% agar) plus Te from −80°C stocks and left for 5 days in the anaerobic glove box (Jacomex) with an oxygen concentration of 2 ppm; colonies from these plates were used to inoculate pre-cultures. For the strains overexpressing the *APN1* and *NTG1* genes, SD without uracil was the reference medium used for liquid cultures and plating.

TUNEL assay and ROS measurements by flow cytometry

Liquid cultures in SDTe were inoculated at $OD_{600nm} \sim 0.1$ from an overnight anaerobic pre-culture and grown for 14 h to an $OD_{600nm} \sim 1$. Cultures were exposed to air for various times, and aliquots of 10^7 cells were centrifuged and immediately reintroduced into the anaerobic glove box. DNA-strand breaks were detected by terminal deoxynucleotidyl transferase-mediated dUTP nick-end labeling (TUNEL assay) using the *in situ* cell death detection kit, fluorescein (Roche Diagnostics). After anaerobic to aerobic transition, cells were fixed with 4% formaldehyde in PBS (137 mM NaCl, 2.7 mM KCl, 10 mM sodium phosphate dibasic, 2 mM potassium phosphate monobasic, pH 7.4) for 1–4 h and the cell wall was digested with 20 μl β-glucuronidase/arylsulfatase (Roche Diagnostics) and 5 U lyticase (Sigma) for 1.5 h at 30°C. Spheroplasts were permeabilized with 0.1% Triton X-100 and labeled following the manufacturer's instructions for the kit. For staining in aerobic conditions, exponential cells ($OD_{600nm} \sim 0.4$) were cultivated 4 h with and without 5 mM PBN before fixation and labeling. Samples were analyzed by flow cytometry using a CyAn ADP 9C apparatus (Beckman Coulter) with excitation at 488 nm and emission detection through a 530/40 nm band pass filter (fluorescein).

Intracellular free radicals were detected using DHE (Sigma-Aldrich Co) and analyzed by flow cytometry with excitation and emission settings of 488 and 613/620 nm. For DHE staining during the anaerobic to aerobic transition, cells were labeled with 2.5 μg/ml of dihydroethydium in PBS for 15 min in anaerobiosis. For DHE staining in aerobic conditions, 5 μg/ml DHE were added to log-phase cell cultures ($OD_{600nm} \sim 0.4$) and the cells were grown for a further 2 h in the dark, centrifuged, resuspended in PBS buffer and analyzed. Data were analyzed and quantified as previously reported (21).

Illegitimate mating and loss of mitochondrial DNA

The same haploid strains were used as mating-type and ρ^- tester strains (*Mat*a ρ^0 *thr1* and *Mat*α ρ^0 *thr1*). For illegitimate mating strains, 10^7 cells of the tester strain were spread onto dropout base media (DOB; yeast nitrogen base, ammonium sulfate, 2% D-glucose) plates. After drying, 50 μl drops containing 10^8 cells of wild-type and Δ*yfh1* mutant were added and plates were incubated for 2–3 days at 30°C. To evaluate mitochondrial DNA integrity, haploid tester strain and wild-type or Δ*yfh1* strains were streaked together in the same DOB plate and incubated 3 days at 30°C. Isolated diploid colonies were streaked in YP-2% glycerol plates and replica-plated onto YPD plates. After 3 days at 30°C, the number of colonies capable of growing on glycerol media was counted.

Spontaneous Can^R mutation frequencies

Spontaneous mutagenesis was monitored by forward mutation in the *CAN1* gene that leads to inactivation of the encoded protein, arginine permease and canavanine resistance. For each strain, one isolated colony was inoculated into 5 ml SDTe and grown for 3 days in anaerobiosis or aerobiosis. Cell density was measured by plating appropriate dilutions into YPD or SD-uracil plates and counting the colonies after 3–5 days at 30°C. The quantification of canavanine-resistant mutants (Can^R) was assayed by plating the cell culture in SD without arginine plates containing 60 mg/l of L-canavanine (Sigma) and counting the colonies after 5–8 days at 30°C. All experiments were repeated at least three times. Mutation frequency was calculated as the number of Can^R mutants per 10^7 surviving cells (data presented in Figs 3B and 4A and B).

O_2-, H_2O_2- and MMS-induced mutation frequencies

Cells grown overnight in SD media were diluted to an OD_{600nm} of 0.1, or 0.2 for Δ*yfh1* mutants, and allowed to grow for 5 h ($\sim 5 \times 10^6$ cells/ml) in anaerobiosis for transition to aerobiosis experiments or in aerobiosis for H_2O_2 or MMS treatments. Aliquots were transferred to aerobiosis or challenged for 30 min with H_2O_2 and MMS at 30°C. Cell density was measured by plating appropriate dilutions into YPD or SD-uracil plates in aerobiosis and counting the colonies after 3–5 days at 30°C. To screen Can^R mutants, cells were plated onto SD without arginine plates containing 60 mg/l of L-canavanine in aerobiosis and the colonies counted after 5–10 days at 30°C. Mutation frequency was calculated as the number of Can^R mutants per 10^7 surviving cells.

Cell cycle analysis by multispectral imaging flow cytometry

Cell cycle progression was analyzed using the ImageStream^X imaging flow cytometer system (Amnis), which combines the advantage of analyzing large numbers of cells by flow cytometry while simultaneously acquiring image data from individual cells. The preparation of asynchronized populations of cells for SYTOX Green (Invitrogen) staining was performed as described (39). Briefly, overnight grown cultures in anaerobiosis or aerobiosis in SDTe were diluted to an $OD_{600nm} \sim 0.3$ and allowed to reach $OD_{600nm} \sim 0.7$ (3–6 h depending on the strain). At this point, anaerobic cultures were shifted to air and cells were collected at 30, 60 and 120 min. The 488 nm laser was used for excitation and fluorescence images using extended depth of field were collected on channel 3 (560–595 nm), and bright-field images were collected on channels 1 and 9. Between 10 000 and 50 000 cells were acquired for statistical analysis. The IDEAS software (Amnis) was used for image analysis. The bivariate plot of the nuclear intensity aspect ratio (ratio of minor axis intensity to major axis intensity) versus the SYTOX Green fluorescence intensity of single focused cells shows the segregation of the cell populations in G1-, S- and G2/M-phases based on nuclear DNA content, and cell and nuclear morphology (39).

RNA isolation and RT-qPCR analysis

Total RNA for RT-qPCR analysis was extracted from cells, cultured in SD media in anaerobiosis to an $OD_{600nm} \sim 1.0$, using the hot phenol method as described previously (34) and purified using QIAGEN columns (RNeasy kit). RT-qPCR analysis was performed exactly as described previously (21,34). Primer pairs used were: 5′-TCGCGTAAGGAACAGTTAGACA-3′ and 5′-GCTCTGCAGTGGCTTTCTTC-3′ for the *APN1* gene; 5′-TAAGGGGCTTTGGACAGAAA-3′ and 5′-ATCATCCGG TGGCAAGAA-3′ for the *NTG1* gene and 5′-CCAGGGGTAA GAGGTGTGATT-3′ and 5′-TCCAATTGATGAAATTTGGA AGA-3′ for the *NTG2* gene or were described previously for the other genes (21,34). Relative expression was calculated using the equation described (53). The results reported were obtained from at least three biological replicates and PCR runs were repeated at least twice.

Determination of glutathione content

Total glutathione levels were determined using a modified version of the recycling enzymatic assay, as previously described (34).

Statistical analysis

All values represent means ± SE for at least biological triplicates ($n \geq 3$). All experiments were repeated at least twice. Statistical analysis was performed using the paired *t*-test.

ACKNOWLEDGEMENTS

We thank Anne-Lise Haenni (IJM) for revising the manuscript.

Conflict of Interest statement. None declared.

FUNDING

This work was supported by the French Government (CNRS), the French FA Patient Organization (AFAF) and the Agence Nationale de la Recherche (ANR Maladies Rares, France). Funding to pay the Open Access publication charges for this article was provided by the French FA Patient Organization (AFAF).

REFERENCES

1. Campuzano, V., Montermini, L., Molto, M.D., Pianese, L., Cossée, M., Cavalcanti, F., Monros, E., Rodius, F., Duclos, F., Monticelli, A. *et al.* (1996) Friedreich's ataxia: autosomal recessive disease caused by an intronic GAA triplet repeat expansion. *Science*, **271**, 1423–1427.
2. Wells, R.D. (2008) DNA triplexes and Friedreich ataxia. *FASEB J.*, **22**, 1625–1634.
3. De Biase, I., Chutake, Y.K., Rindler, P.M. and Bidichandani, S.I. (2009) Epigenetic silencing in Friedreich ataxia is associated with depletion of CTCF (CCCTC-binding factor) and antisense transcription. *PLoS ONE*, **4**, e7914.
4. Stemmler, T.L., Lesuisse, E., Pain, D. and Dancis, A. (2010) Frataxin and mitochondrial FeS cluster biogenesis. *J. Biol. Chem.*, **285**, 26737–26743.
5. Santos, R., Lefevre, S., Sliwa, D., Seguin, A., Camadro, J.M. and Lesuisse, E. (2010) Friedreich ataxia: molecular mechanisms, redox considerations and therapeutic opportunities. *Antioxid. Redox Signal.*, **13**, 651–690.
6. Armstrong, J.S., Khdour, O. and Hecht, S.M. (2010) Does oxidative stress contribute to the pathology of Friedreich's ataxia? A radical question. *FASEB J.*, **24**, 2152–2163.
7. Schmucker, S., Martelli, A., Colin, F., Page, A., Wattenhofer-Donzé, M., Reutenauer, L. and Puccio, H. (2011) Mammalian frataxin: an essential function for cellular viability through an interaction with a preformed ISCU/NFS1/ISD11 iron-sulfur assembly complex. *PLoS ONE*, **6**, e16199.
8. Gakh, O., Bedekovics, T., Duncan, S.F., Smith, D.Y.t., Berkholz, D.S. and Isaya, G. (2010) Normal and Friedreich ataxia cells express different isoforms of frataxin with complementary roles in iron-sulfur cluster assembly. *J. Biol. Chem.*, **285**, 38486–38501.
9. Bridwell-Rabb, J., Iannuzzi, C., Pastore, A. and Barondeau, D.P. (2012) Effector role reversal during evolution: the case of frataxin in Fe-S cluster biosynthesis. *Biochemistry*, **51**, 2506–2514.
10. Bayot, A., Santos, R., Camadro, J.M. and Rustin, P. (2011) Friedreich ataxia: the vicious circle hypothesis revisited. *BMC Med.*, **9**, 112.
11. Svilar, D., Goellner, E.M., Almeida, K.H. and Sobol, R.W. (2011) Base excision repair and lesion-dependent subpathways for repair of oxidative DNA damage. *Antioxid. Redox Signal.*, **14**, 2491–2507.
12. Jeppesen, D.K., Bohr, V.A. and Stevnsner, T. (2011) DNA repair deficiency in neurodegeneration. *Prog. Neurobiol.*, **94**, 166–200.
13. Thierbach, R., Drewes, G., Fusser, M., Voigt, A., Kuhlow, D., Blume, U., Schulz, T.J., Reiche, C., Glatt, H., Epe, B. *et al.* (2010) The Friedreich's ataxia protein frataxin modulates DNA base excision repair in prokaryotes and mammals. *Biochem. J.*, **432**, 165–172.
14. Karthikeyan, G., Lewis, L.K. and Resnick, M.A. (2002) The mitochondrial protein frataxin prevents nuclear damage. *Hum. Mol. Genet.*, **11**, 1351–1362.
15. Karthikeyan, G., Santos, J.H., Graziewicz, M.A., Copeland, W.C., Isaya, G., Van Houten, B. and Resnick, M.A. (2003) Reduction in frataxin causes progressive accumulation of mitochondrial damage. *Hum. Mol. Genet.*, **12**, 3331–3342.
16. Haugen, A.C., Di Prospero, N.A., Parker, J.S., Fannin, R.D., Chou, J., Meyer, J.N., Halweg, C., Collins, J.B., Dürr, A., Fischbeck, K. *et al.* (2010) Altered gene expression and DNA damage in peripheral blood cells from Friedreich's ataxia patients: cellular model of pathology. *PLoS Genet.*, **6**, e1000812.
17. Wilson, R.B. and Roof, D.M. (1997) Respiratory deficiency due to loss of mitochondrial DNA in yeast lacking the frataxin homologue. *Nat. Genet.*, **16**, 352–357.

18. Babcock, M., de Silva, D., Oaks, R., Davis-Kaplan, S., Jiralerspong, S., Montermini, L., Pandolfo, M. and Kaplan, J. (1997) Regulation of mitochondrial iron accumulation by Yfh1p, a putative homolog of frataxin. *Science*, **276**, 1709–1712.
19. Foury, F. and Cazzalini, O. (1997) Deletion of the yeast homologue of the human gene associated with Friedreich's ataxia elicits iron accumulation in mitochondria. *FEBS Lett.*, **411**, 373–377.
20. Bradley, J.L., Blake, J.C., Chamberlain, S., Thomas, P.K., Cooper, J.M. and Schapira, A.H. (2000) Clinical, biochemical and molecular genetic correlations in Friedreich's ataxia. *Hum. Mol. Genet.*, **9**, 275–282.
21. Lefevre, S., Sliwa, D., Auchère, F., Brossas, C., Ruckenstuhl, C., Boggetto, N., Lesuisse, E., Madeo, F., Camadro, J.M. and Santos, R. (2012) The yeast metacaspase is implicated in oxidative stress response in frataxin-deficient cells. *FEBS Lett.*, **586**, 143–148.
22. Seguin, A., Bayot, A., Dancis, A., Rogowska-Wrzesinska, A., Auchère, F., Camadro, J.M., Bulteau, A.L. and Lesuisse, E. (2009) Overexpression of the yeast frataxin homolog (Yfh1): contrasting effects on iron-sulfur cluster assembly, heme synthesis and resistance to oxidative stress. *Mitochondrion*, **9**, 130–138.
23. Anderson, P.R., Kirby, K., Orr, W.C., Hilliker, A.J. and Phillips, J.P. (2008) Hydrogen peroxide scavenging rescues frataxin deficiency in a *Drosophila* model of Friedreich's ataxia. *Proc. Natl Acad. Sci. USA*, **105**, 611–616.
24. Paupe, V., Dassa, E., Goncalves, S., Auchère, F., Lönn, M., Holmgren, A. and Rustin, P. (2009) Impaired nuclear Nrf2 translocation undermines the oxidative stress response in Friedreich ataxia. *PLoS ONE*, **4**, e4253.
25. Gros, L., Saparbaev, M.K. and Laval, J. (2002) Enzymology of the repair of free radicals-induced DNA damage. *Oncogene*, **21**, 8905–8925.
26. Boiteux, S. and Guillet, M. (2004) Abasic sites in DNA: repair and biological consequences in *Saccharomyces cerevisiae*. *DNA Repair (Amst)*, **3**, 1–12.
27. Alseth, I., Eide, L., Pirovano, M., Rognes, T., Seeberg, E. and Bjørås, M. (1999) The *Saccharomyces cerevisiae* homologues of endonuclease III from *Escherichia coli*, Ntg1 and Ntg2, are both required for efficient repair of spontaneous and induced oxidative DNA damage in yeast. *Mol. Cell Biol.*, **19**, 3779–3787.
28. Swartzlander, D.B., Griffiths, L.M., Lee, J., Degtyareva, N.P., Doetsch, P.W. and Corbett, A.H. (2010) Regulation of base excision repair: Ntg1 nuclear and mitochondrial dynamic localization in response to genotoxic stress. *Nucleic Acids Res.*, **38**, 3963–3974.
29. Gregor, I. and Tsugita, A. (1982) The amino acid sequence of cytochrome c oxidase subunit VI from *Saccharomyces cerevisiae*. *J. Biol. Chem.*, **257**, 13081–13087.
30. Popoff, S.C., Spira, A.I., Johnson, A.W. and Demple, B. (1990) Yeast structural gene (*APN1*) for the major apurinic endonuclease: homology to *Escherichia coli* endonuclease IV. *Proc. Natl Acad. Sci. USA*, **87**, 4193–4197.
31. Vongsamphanh, R., Fortier, P.K. and Ramotar, D. (2001) Pir1p mediates translocation of the yeast Apn1p endonuclease into the mitochondria to maintain genomic stability. *Mol. Cell Biol.*, **21**, 1647–1655.
32. Acevedo-Torres, K., Fonseca-Williams, S., Ayala-Torres, S. and Torres-Ramos, C.A. (2009) Requirement of the *Saccharomyces cerevisiae APN1* gene for the repair of mitochondrial DNA alkylation damage. *Environ. Mol. Mutagen.*, **50**, 317–327.
33. Bulteau, A.L., Dancis, A., Gareil, M., Montagne, J.J., Camadro, J.M. and Lesuisse, E. (2007) Oxidative stress and protease dysfunction in the yeast model of Friedreich ataxia. *Free Radic. Biol. Med.*, **42**, 1561–1570.
34. Auchère, F., Santos, R., Planamente, S., Lesuisse, E. and Camadro, J.M. (2008) Glutathione-dependent redox status of frataxin-deficient cells in a yeast model of Friedreich's ataxia. *Hum. Mol. Genet.*, **17**, 2790–2802.
35. Madeo, F., Fröhlich, E., Ligr, M., Grey, M., Sigrist, S.J., Wolf, D.H. and Fröhlich, K.U. (1999) Oxygen stress: a regulator of apoptosis in yeast. *J. Cell Biol.*, **145**, 757–767.
36. Hicks, W.M., Yamaguchi, M. and Haber, J.E. (2011) Real-time analysis of double-strand DNA break repair by homologous recombination. *Proc. Natl Acad. Sci. USA*, **108**, 3108–3115.
37. Rasmussen, A.K., Chatterjee, A., Rasmussen, L.J. and Singh, K.K. (2003) Mitochondria-mediated nuclear mutator phenotype in *Saccharomyces cerevisiae*. *Nucleic Acids Res.*, **31**, 3909–3917.
38. Putnam, C.D., Jaehnig, E.J. and Kolodner, R.D. (2009) Perspectives on the DNA damage and replication checkpoint responses in *Saccharomyces cerevisiae*. *DNA Repair (Amst.)*, **8**, 974–982.
39. Calvert, M.E. and Lannigan, J. (2010) Yeast cell cycle analysis: combining DNA staining with cell and nuclear morphology. *Curr. Protoc. Cytom.*, Chapter 9, Unit 9.32.1–16.
40. Calvert, M.E., Lannigan, J.A. and Pemberton, L.F. (2008) Optimization of yeast cell cycle analysis and morphological characterization by multispectral imaging flow cytometry. *Cytometry A*, **73**, 825–833.
41. Veatch, J.R., McMurray, M.A., Nelson, Z.W. and Gottschling, D.E. (2009) Mitochondrial dysfunction leads to nuclear genome instability via an iron-sulfur cluster defect. *Cell*, **137**, 1247–1258.
42. Díaz de la Loza, M.C., Gallardo, M., García-Rubio, M.L., Izquierdo, A., Herrero, E., Aguilera, A. and Wellinger, R.E. (2011) Zim17/Tim15 links mitochondrial iron-sulfur cluster biosynthesis to nuclear genome stability. *Nucleic Acids Res.*, **39**, 6002–6015.
43. Lesuisse, E., Santos, R., Matzanke, B.F., Knight, S.A., Camadro, J.M. and Dancis, A. (2003) Iron use for haeme synthesis is under control of the yeast frataxin homologue (Yfh1). *Hum. Mol. Genet.*, **12**, 879–889.
44. Yoon, H., Golla, R., Lesuisse, E., Pain, J., Donald, J.E., Lyver, E.R., Pain, D. and Dancis, A. (2012) Mutation in the Fe-S scaffold protein Isu bypasses frataxin deletion. *Biochem. J.*, **441**, 473–480.
45. Kitanovic, A., Walther, T., Loret, M.O., Holzwarth, J., Kitanovic, I., Bonowski, F., Van Bui, N., Francois, J.M. and Wölfl, S. (2009) Metabolic response to MMS-mediated DNA damage in *Saccharomyces cerevisiae* is dependent on the glucose concentration in the medium. *FEMS Yeast Res.*, **9**, 535–551.
46. Wu, Y. and Brosh, R.M.J. (2012) DNA helicase and helicase-nuclease enzymes with a conserved iron-sulfur cluster. *Nucleic Acids Res.*, doi:10.1093/nar/gks039.
47. Luo, M., He, H., Kelley, M.R. and Georgiadis, M.M. (2010) Redox regulation of DNA repair: implications for human health and cancer therapeutic development. *Antioxid. Redox Signal.*, **12**, 1247–1269.
48. Tell, G., Quadrifoglio, F., Tiribelli, C. and Kelley, M.R. (2009) The many functions of APE1/Ref-1: not only a DNA repair enzyme. *Antioxid. Redox Signal.*, **11**, 601–620.
49. Vasko, M.R., Guo, C. and Kelley, M.R. (2005) The multifunctional DNA repair/redox enzyme Ape1/Ref-1 promotes survival of neurons after oxidative stress. *DNA Repair (Amst.)*, **4**, 367–379.
50. Zhang, Y., Lyver, E.R., Knight, S.A., Lesuisse, E. and Dancis, A. (2005) Frataxin and mitochondrial carrier proteins, Mrs3p and Mrs4p, cooperate in providing iron for heme synthesis. *J. Biol. Chem.*, **280**, 19794–19807.
51. Longtine, M.S., McKenzie, A.r., Demarini, D.J., Shah, N.G., Wach, A., Brachat, A., Philippsen, P. and Pringle, J.R. (1998) Additional modules for versatile and economical PCR-based gene deletion and modification in *Saccharomyces cerevisiae*. *Yeast*, **14**, 953–961.
52. Mumberg, D., Müller, R. and Funk, M. (1995) Yeast vectors for the controlled expression of heterologous proteins in different genetic backgrounds. *Gene*, **156**, 119–122.
53. Pfaffl, M.W. (2001) A new mathematical model for relative quantification in real-time RT-PCR. *Nucleic Acids Res.*, **29**, e45–e50.